How to Cite: Kumari, S., Gupta, P. K., Kumar, A., & Kumar, R. (2025). Oxidative Transformation of Ethylbenzene Utilizing Metal Bound Immobilized Catalysts. *Eurasian Journal of Chemistry, 30, 4(120), 120–136.* https://doi.org/10.31489/2959-0663/4-25-2

Article

Received: 20 May 2025 | Revised: 28 November 2025 |
Accepted: 5 December 2025 | Published online: 12 December 2025

UDC 544.42+519.242.7

https://doi.org/10.31489/2959-0663/4-25-2

Savita Kumari[1], Praveen K. Gupta[1*], Amit Kumar[2], Ramesh Kumar[3]

[1]*Department of Chemistry, Maharishi Markandeshwar (Deemed to be University), Haryana, India;*
[2]*Department of Chemistry, Indira Gandhi National College, Haryana, India;*
[3]*Department of Chemistry, Kurukshetra University, Haryana, India*
*(*Corresponding author's e-mail: praveenguptachem@gmail.com; parveen.gupta@mmumullana.org)*

Oxidative Transformation of Ethylbenzene Utilizing Metal Bound Immobilized Catalysts

In the present contribution, we have investigated the catalytic potential of immobilized metal catalysts for the oxidation of ethylbenzene. Chloromethylated polystyrene was initially converted to aldehydopolystyrene followed by its functionalization with 2-aminothiophenol to get functionalized resin. This resin was successfully binded with appropriate metal (Mn(II), Fe(III), Ni(II), Cu(II), VO(II)) salts to prepare different heterogeneous catalysts which were characterized using CHNS, energy dispersive X-ray spectroscopy (EDX), diffuse reflectance spectra (DRS), fourier transform infrared spectra (FTIR), atomic absorption spectrophotometry (AAS) and electron paramagnetic resonance (EPR) spectra techniques. Metal binding in mmol per gram of resin for different catalysts was found in the range 0.96–1.24. The catalytic potential of these supported catalysts was assessed for the oxidation of ethylbenzene, utilizing hydrogen peroxide (H_2O_2) and tert-butyl hydroperoxide (TBHP) as the oxidants. The effects of various reaction parameters, such as temperature, reaction duration, type of oxidant, and the amount of catalyst used were examined for the oxidation reaction. Under optimized milder conditions, the results showed that H_2O_2 as oxidants resulted in 53.8 % conversion rates with the copper catalyst. The nickel catalyst, when used with H_2O_2, showed the highest selectivity for acetophenone, reaching 83 %. The recovered catalysts retained its original structure, as established by a comparative analysis of DRS and FT-IR spectra of both the original and reused catalysts. Moreover, the catalysts can be employed repeatedly up to five times under optimum conditions without any noticeable reduction in activity.

Keywords: immobilization, catalyst, nickel, copper, recycle, oxidation, ethylbenzene, polymer

Introduction

Catalysis indeed plays a crucial role in modern chemistry, serving as a cornerstone for sustainable and efficient chemical transformations. By accelerating reactions, catalysts allow the synthesis of valuable products under milder conditions [1]. Transition metal based catalysts are indeed powerful, widely used in a variety of chemical transformations like hydrocarboxylation and hydroesterification reaction, olefin polymerization, carbonylation of propargylic and allylic compounds, isomerization of olefin, cross-coupling reactions, C–N and C–O bond-forming reactions, olefinations of aryl halides, olefin metathesis and many other key reactions in industry [2, 3]. Their adaptability and high efficiency make them indispensable in modern synthetic chemistry. Polystyrene-anchored transition metal complexes represent an important class of heterogeneous catalysts due to their stability and versatility in catalyzing a range of organic transformations [4]. These complexes are often chemically inert, preventing unwanted side reactions, and can be reused in multiple reaction cycles without significant loss of activity, making them both economically and environmentally favorable [5]. Unlike homogeneous catalysts that are dissolved in the reaction medium, supported catalysts are often heterogeneous (insoluble), which allows them to be separated by simple filtration or centrifugation. This significantly simplifies the post-reaction purification process [6]. Polystyrene supports can be chemically modified into other functional supports, such as aldehyde, carboxylic acid, acid chloride, aminomethylated and azidomethyl resins [7]. This adaptability allows fine-tuning of the polymer's reactivity and its ability to bind different metal catalysts, broadening its application to various catalytic processes [8–10]. These catalysts not only enhance the reaction's stability and selectivity but also make the process more sustainable due to their reusability and the use of eco-friendly oxidants. The oxidation of ethylbenzene in the presence of polymer-anchored catalysts can produce a range of products, including acetophenone, benzaldehyde, and benzoic acid. In a similar manner, acetophenone, an important product derived from the selective oxidation of ethylbenzene [11], has attracted significant interest. It is widely used as an intermediate in pharmaceuticals, aldehydes, resins, alcohols, esters, tear gas formulations, and also finds applications in perfumery and sleep-

inducing drugs [12–16]. Benzaldehyde's versatility makes it an important compound in various sectors, from flavors and fragrances to pharmaceuticals and industrial applications. Its distinctive odor and chemical reactivity contribute to its broad range of uses [17–20]. Benzoic acid and its salts, such as sodium benzoate, are widely used as preservatives in food and beverages, cosmetics, intermediate, dyes and pigments etc. [21, 22].

Several studies have reported efficient catalytic systems for the oxidation of ethylbenzene using various oxidants. Faraji et al. achieved 88.1 % conversion and 98 % selectivity to acetophenone with reusable amino propyl trimethoxysilane immobilized metformin-cobalt nanocatalyst [Fe_3O_4@SiO_2-APTMS/CC/Met@Co(II)] using O_2/N-hydroxyphthalimide (NHPI) as an oxidant at 100 °C [23]. Gao et al. employed Co_3O_4 nanoparticles supported on reduced graphene oxide (Co/rGO) with O_2/NHPI, affording 84.1 % conversion and 96.2 % selectivity in 2 h at 120 °C [24]. Li et al. developed a Co-based single-atom black powdered catalyst anchored on a graphitic carbon nitride (SACo@g-C_3N_4) with peroxymonosulfate (PMS) as oxidant, yielded over 95 % conversion and selectivity under mild conditions [25]. Yang et al. reported Mn(II) complexes bearing bis(pyridin-2-ylmethyl)amine ligands that oxidized ethylbenzene with ozone (O_3) in an acetonitrile-water (1:1) medium to give 91 % conversion and 89 % selectivity [26]. Similarly, Yamazaki et al. demonstrated complete conversion (100 %) using CrO_3 and periodic acid (H_5IO_6) as oxidant at room temperature, affording 49 % acetophenone selectivity within 1 h [27]. The aim of this study was to describe the series of new immobilized catalysts, provide their structural characterization, and demonstrate their application for the selective oxidation of ethylbenzene using H_2O_2 and TBHP as an oxidants.

Experimental

Materials and Methods

2-aminothiophenol (99 % purity, Sigma-Aldrich), chloromethylated polystyrene (2 % divinylbenzene cross-linked, 4.5 mmol Cl/g of resin, mesh 200–400) was generously gifted by Thermax Ltd, Pune, India. All other reagents were purchased from Central Drug House (CDH). Nickel(II) chloride hexahydrate ($NiCl_2{\cdot}6H_2O$, ≥98 %, AR grade), iron(III) chloride hexahydrate ($FeCl_3{\cdot}6H_2O$, 98 %, AR grade), copper(II) chloride dihydrate ($CuCl_2{\cdot}2H_2O$, 99 %, AR grade), manganese(II) acetate tetrahydrate [$Mn(CH_3COO)_2{\cdot}4H_2O$, 99.5 %, AR grade], vanadyl sulphate pentahydrate ($VOSO_4{\cdot}6H_2O$, 97 %, AR grade), 2,4-dinitrophenylhydrazine reagent (99 %, AR grade), hydrogen peroxide (H_2O_2, 30 % in water), *t*-butyl hydroperoxide [$(CH_3)_3COOH$, 70 % in water], ethylbenzene (98 %, synthesis grade), acetonitrile (CH_3CN, 99 %, AR grade), methanol (CH_3OH, 99 %, synthesis grade), ethanol (C_2H_5OH, 99 %, synthesis grade) and acetone [$(CH_3)_2O$, 99 %, synthesis grade] were used for the synthesis. Analytical-grade reagents were dried according to the standard procedures without any further purification.

The synthesized compounds were analyzed using a range of techniques, including FT-IR, DRS, ESR, EDS, AAS, and CHNS elemental analysis. FT-IR spectra were recorded from 400 to 4000 cm^{-1} on a Shimadzu IR Spirit Fourier transform infrared spectrophotometer. Diffuse reflectance spectra (DRS) were obtained using a Shimadzu UV-2600 double beam spectrophotometer with $BaSO_4$ as the standard. CHNS analysis was conducted using a Thermo Scientific Flash 2000 analyzer. Metal content in the polymer-anchored catalysts was measured titrimetrically and gravimetrically as well as with a Shimadzu ASC-6880 atomic absorption spectrophotometer (AAS). Energy dispersive X-ray (EDX) spectra were captured with a Hitachi SU8010 Series FEG scanning electron microscope. Electron paramagnetic resonance (EPR) spectra were recorded on JES-FA200 X-band (9.45 GHz) spectrometer with a modulation frequency of 100 kHz and modulation amplitude of 2.0 Gauss. Gas Chromatography-Mass Spectrometry (GC-MS) analysis was performed using an Agilent 7000 GC/TQ system. The gas chromatograph used was equipped with GsBP-624 column and FID detector.

Synthesis of Aldehydopolystyrene (PS-CHO)

Chloromethylated polystyrene beads (6 g) were swollen in 100 mL of DMSO for an hour. Sodium hydrogen carbonate (7.5 g) was then added, and the mixture was stirred and refluxed at 150 °C for 6 hours. The resulting aldehyde-functionalized polymer was isolated by vacuum filtration, washed with ethanol, and dried in a vacuum desiccator at 25 °C.

Functionalization of Aldehydopolystyrene with 2-Aminothiophenol [PS-ATP]

PS-CHO beads (6 g) were first allowed to swell in 30 mL of methanol for an hour. Separately, 2-aminothiophenol (ATP) (30 mmol) was dissolved in 50 mL of methanol and then introduced into the polymer suspension. The reaction mixture was stirred and refluxed at 80 °C in a water bath for 18 hours. After completion, the solid was collected by vacuum filtration and repeatedly washed with hot ethanol, hot metha-

nol, and acetone. The final product was dried in an air oven at 70 °C. The addition of the ligand to the polymer was periodically monitored using the 2,4-DNP test.

Loading of Metal to Functionalized Aldehydopolystyrene Resin

The functionalized resin PS-ATP (4.5 mmol) was initially swollen in 15 mL of methanol for an hour. A metal salt solution was prepared by dissolving $VOSO_4 \cdot 5H_2O$, $Mn(CH_3COO)_2 \cdot 4H_2O$, $FeCl_3 \cdot 6H_2O$, $NiCl_2 \cdot 6H_2O$ or $CuCl_2 \cdot 2H_2O$ (4.5–9.0 mmol) in methanol, which was then introduced into the resin suspension. As the reaction proceeded, a noticeable color change was observed in the resin. The mixture was subjected to reflux for 6–18 hours, and then allowed to cool to room temperature. The solid was collected via vacuum filtration and thoroughly washed with hot methanol, ethanol, and acetone. Finally, the resin was dried in an oven at 80 °C.

Experiment on Catalytic Performance

Ethylbenzene oxidation using catalysts was performed in a thermostatted oil bath. The reaction was carried out with *tert*-butyl hydroperoxide/or hydrogen peroxide as oxidants at 60 °C for 3–8 hours, using catalyst amounts of 0.1 and 0.15 g. The catalyst was pre-swollen in 20 mL of acetonitrile for 30 minutes before adding ethylbenzene (10 mmol) and the oxidant (20 mmol). The reaction was monitored via TLC, and product formation was confirmed by GC-MS. A control experiment without the catalyst was also conducted. The catalyst was recovered, washed, dried under vacuum, and reused.

Results and Discussion

The aldehydopolystyrene was modified with 2-aminothiophenol to form the functionalized resin [PS-ATP] **(**Fig. 1). Ligands at the para position of the polymer backbone facilitated metal binding (Fig. 3). The formation of immobilized metal catalysts (Fig. 2) was initially observed through a change in colour of the beads and later confirmed by characterization techniques. The ligand attachment was verified by the DNP test, where the disappearance of the orange color indicated aldehyde group replacement (Fig. 4(*a*)). Real images of the functionalized resin and its metal catalysts are shown in (Fig. 4(*b-g*)).

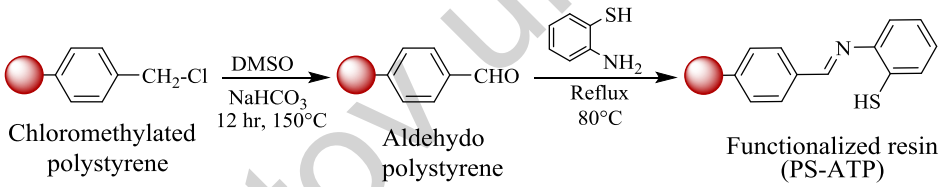

Figure 1. Synthesis of polystyrene-anchored ligand

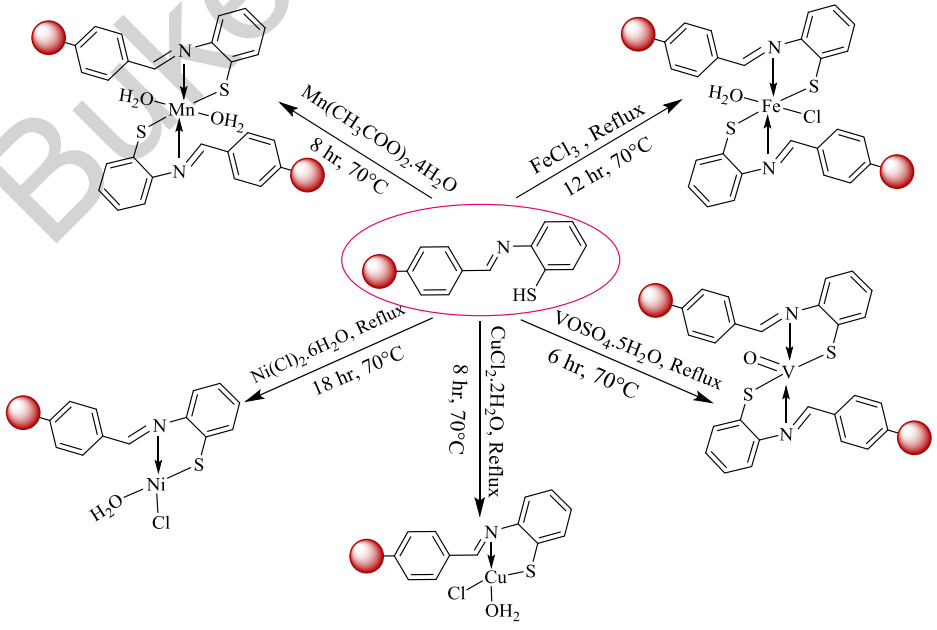

Figure 2. Synthesis of metal incorporated functionalized resin

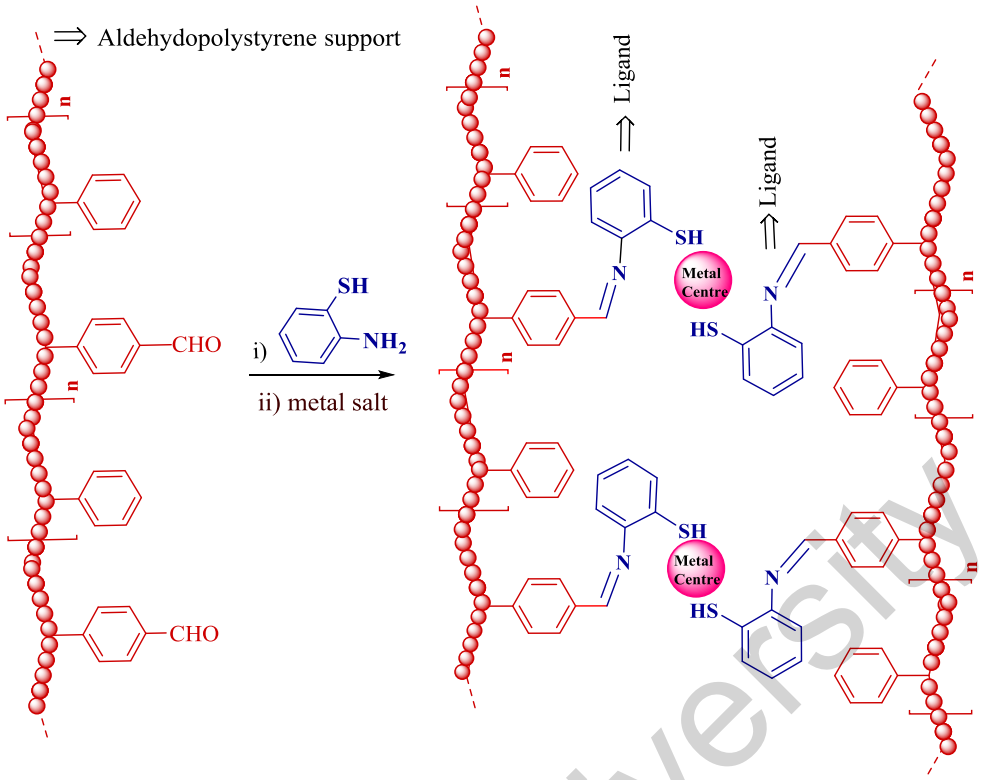

Figure 3. Incorporated metal ions onto functionalized aldehydopolystyrene

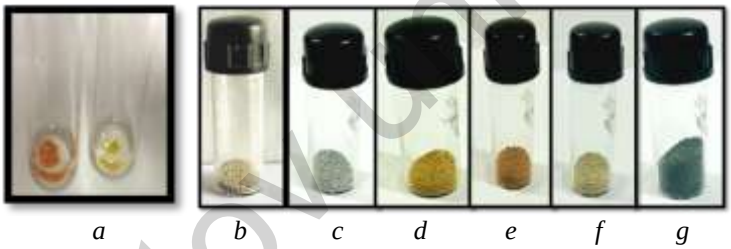

Figure 4. DNP test of [PS-CHO] & [PS-ATP] (*a*); Sample pictures of [PS-ATP] (*b*), [PS-ATP-V] (*c*), [PS-ATP-Mn] (*d*), [PS-ATP-Fe] (*e*), [PS-ATP-Ni] (*f*), [PS-ATP-Cu] (*g*)

Characterization

The incorporation of the organic ligand onto the polymer backbone was confirmed by CHNS analysis through the measurement of carbon, hydrogen, nitrogen, and sulfur content. Metal loading in the catalysts was determined using atomic absorption spectroscopy (AAS) indicating the metal bounded onto the functionalized resin (Table 1), providing insights into the ligand: metal stoichiometry within the polymer structure.

Table 1

Analytical data of functionalized resin and its catalyst

Compound	Colour	Elemental analysis, %					Ligand attachment (mmol per gram of resin)	Metal binding (mmol per gram of resin)	Ligand/ Metal ratio
		C	H	N	S	M			
[PS-ATP]	Cream	80.95	6.92	3.89	8.42	-	2.78	–	–
[PS-ATP-V]	Olive green	72.54	6.71	3.20	8.82	5.9	2.29	1.16	1.97:1
[PS-ATP-Mn]	Mustard	72.91	6.96	2.74	8.99	5.3	1.96	0.96	2:1
[PS-ATP-Fe]	Dark brown	71.65	6.49	3.20	5.89	6.7	2.29	1.19	1.92:1
[PS-ATP-Ni]	Off-white	66.73	6.20	2.05	8.73	7.1	1.46	1.18	1.2:1
[PS-ATP-Cu]	Dark green	65.98	6.19	2.01	8.70	7.9	1.44	1.24	1.2:1

EDX Investigation

EDX analysis confirmed the successful binding of metal ions in all catalysts by detecting their respective ion signals. The spectra for Cu, Fe, and Ni catalysts displayed Cl signals, while the V catalyst exhibited an S signal, indicating coordination with chlorine and sulfur atoms, respectively (Fig. 5).

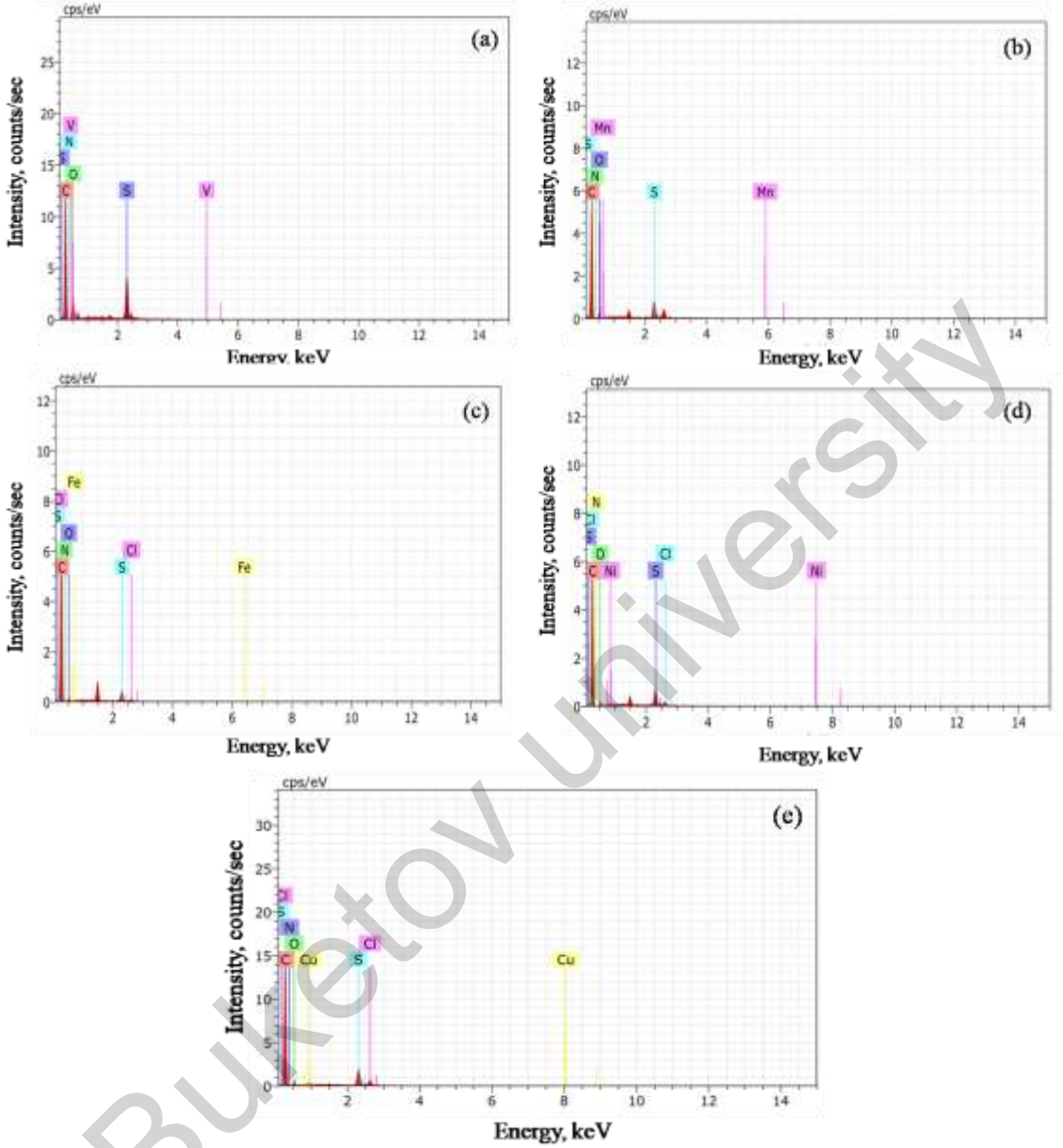

Figure 5. EDX plot of [PS-ATP-V] (*a*), [PS-ATP-Mn] (*b*), [PS-ATP-Fe] (*c*), [PS-ATP-Ni] (*d*) and [PS-ATP-Cu] (*e*)

FTIR Investigation

The binding of metal ions to the polymer support was analysed by FTIR spectra (Fig. 6 and Table 2) of the functionalized resin and its metal catalysts. PS-ATP exhibits a distinct band at 1659 cm^{-1}, corresponding to the ν(C=N) stretch. A shift of 11–21 cm^{-1} to lower wavenumber in this band indicates the coordination of the azomethine nitrogen to the metal ions [28]. The IR spectrum of the functionalized resin shows a weak band at 2571 cm^{-1} which is assigned to the SH group respectively. The disappearance of this band in the spectra of the catalysts indicates the deprotonation of the thiol groups upon chelation [29]. The vanadium catalyst displays a prominent band at 952 cm^{-1} assigned to (V=O) stretch [30]. The interaction of metal ions with [PS-ATP] was confirmed by the appearance of M–N, M–O, and M–S bands in the regions of 486–531 cm^{-1}, 564–572 cm^{-1}, and 423–449 cm^{-1}, respectively [31]. A band in the region 3312–3415 cm^{-1} in the metal catalysts indicates the coordination of a water molecule [32].

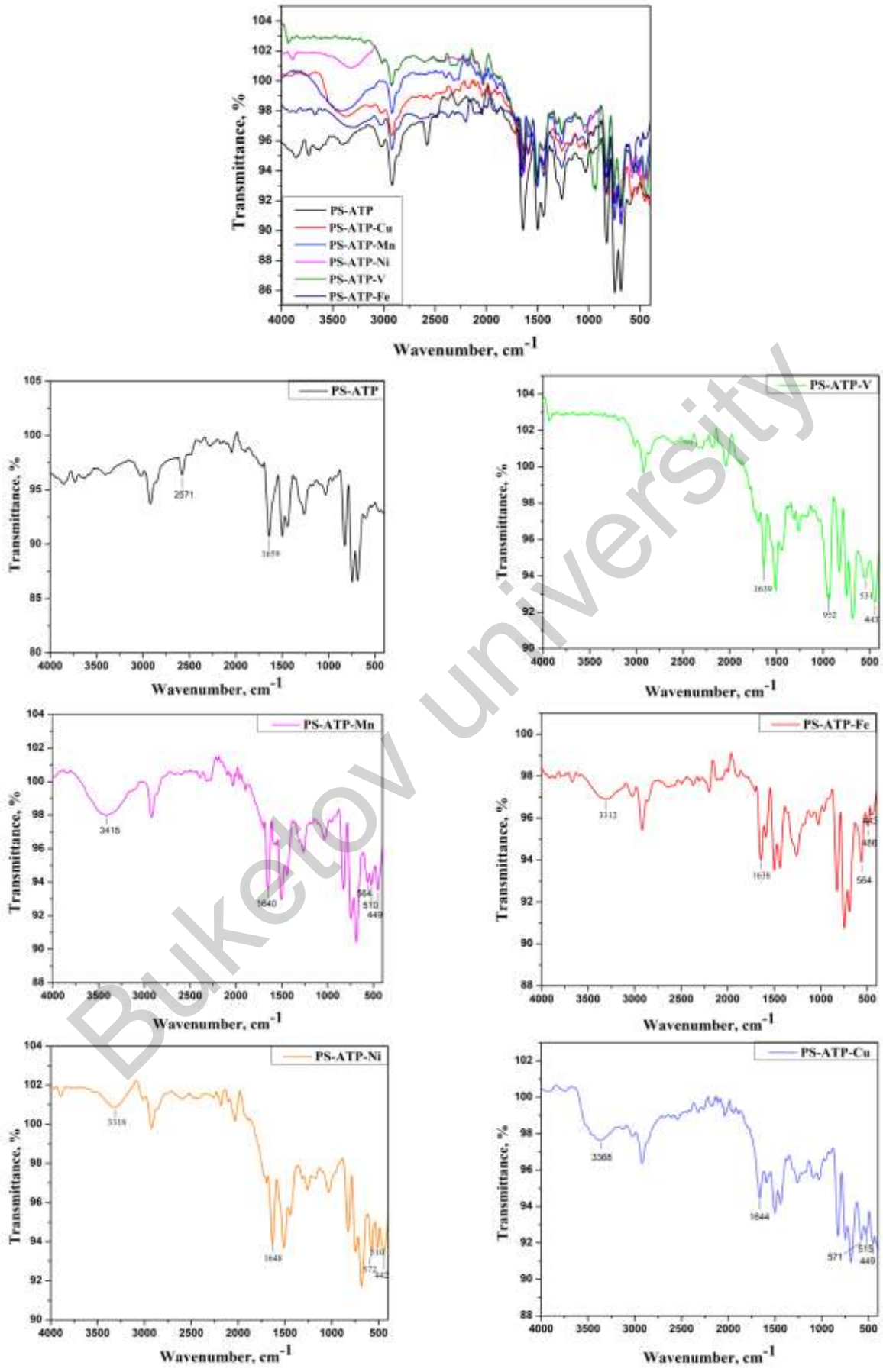

Figure 6. Overlap and individual FTIR spectra of functionalized resin and its metal catalysts

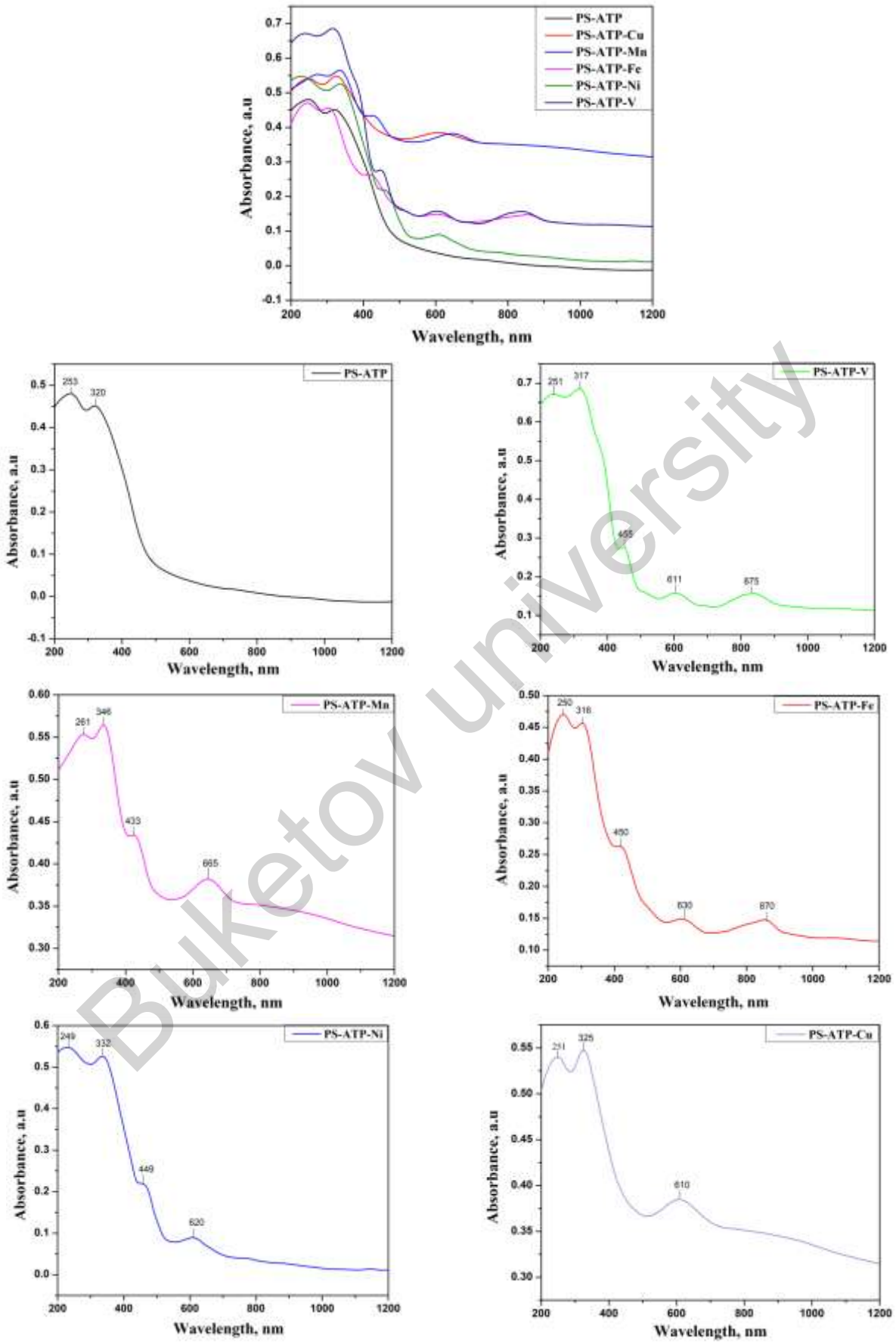

Figure 7. Overlap and individual DRS spectra of metal catalysts

DRS Investigation

Diffuse reflectance spectral studies (Fig. 7, Table 2) were performed to examine the structure of the solid, insoluble catalysts. The [PS-ATP] spectrum shows intraligand absorption transitions and 30303 and 39062 cm^{-1}, corresponding to $n \rightarrow \pi^*$ and $\pi \rightarrow \pi^*$ transitions, respectively. The [PS-ATP-V] spectrum displays three well-resolved transitions at 11428, 16366, and 21978 cm^{-1}, consistent with the spectral characteristics of five-coordinate oxovanadium(IV) complexes possessing C_{4v} symmetry. These three observed transitions can be attributed to $^2B_{2g} \rightarrow {}^2E_g$, $^2B_{2g} \rightarrow {}^2B_{1g}$ and $^2B_{2g} \rightarrow {}^2A_{1g}$ in increasing energy [33]. Manganese shows two bands at 15037 and 23094 cm^{-1}, corresponding to $^6A_{1g} \rightarrow {}^4T_{1g}(G)$ and $^6A_{1g} \rightarrow {}^4T_{2g}(G)$ transitions, suggesting an octahedral geometry [34]. Iron catalyst displays distinct bands at 11494, 15873, and 22222 cm^{-1} due to $^6A_{1g} \rightarrow {}^4T_{1g}(G)(\nu_1)$; $^6A_{1g} \rightarrow {}^4T_{2g}(F)$ (ν_2) and $^6A_{1g} \rightarrow {}^4T_{1g}(P)$ (ν_3) transitions respectively [35]. [PS-ATP-Ni] exhibits spin-allowed transitions at 16129 and 22,271 cm^{-1}, which correspond to $^3A_{2g} \rightarrow {}^3T_{2g}(G)(\nu_1)$ and $^3A_{2g} \rightarrow {}^3T_{1g}(F)(\nu_2)$ transitions, respectively, indicating Ni(II) in an octahedral environment [36]. The reflectance spectrum of copper catalyst shows d → d transitions at 16393 cm^{-1}, which can be attributed to $^2B_{1g} \rightarrow {}^2A_{1g}$; $^2B_{1g} \rightarrow {}^2B_{2g}$; $^2B_{1g} \rightarrow {}^2E_g$ transitions, indicative of a square planar geometry [37].

Table 2

FTIR and DRS spectral data for functionalized resin and its metal catalysts

Polymer-anchored compounds	υ(C=N)	υ(S-H)	υ(V=O)	υ(M-Cl)	υ(H_2O)	d-d band position (cm^{-1})	d-d band assignment
[PS-ATP]	1659	2571	–	–	–	-	-
[PS-ATP-V]	1639	–	952	–	–	11428;16366; 21978	$^2B_2 \rightarrow {}^2E$; $^2B_1$; $^2A_1$
[PS-ATP-Mn]	1640	–	–	–	3415	15037; 23094	$^6A_{1g} \rightarrow {}^4T_{1g}(G)$; $^4T_{2g}(G)$
[PS-ATP-Fe]	1638	–	–	351	3312	11494; 15873; 22222	$^6A_{1g} \rightarrow {}^4T_{1g}(G)(\nu_1)$; $^4T_{2g}(F)$ (ν_2); $^4T_{1g}(P)(\nu_3)$
[PS-ATP-Ni]	1648	–	–	357	3318	16129; 22271	$^3A_{2g} \rightarrow {}^3T_{2g}(G)(\nu_1)$; $^3T_{1g}(F)(\nu_2)$
[PS-ATP-Cu]	1644	–	–	355	3368	16393	$^2B_{1g} \rightarrow {}^2A_{1g}$; $^2B_{2g}$; ^2E_g

EPR Studies

At ambient conditions, EPR spectroscopy was employed to examine vanadium, manganese, and copper catalysts, as illustrated in Figure 8. The EPR spectrum of the vanadium catalyst [PS-ATP-V] exhibits an axially symmetric signal, a characteristic feature of V(IV) ions. This suggests that the electron distribution around the vanadium ion is anisotropic, favoring a specific orientation. Signals appear in both the perpendicular and parallel regions, highlighting the anisotropic nature of the V(IV) ion's electronic structure. The well-defined hyperfine splitting indicates that vanadium ions are uniformly incorporated into the polystyrene support, with no interactions. The spectrum displays anisotropy, with Hamiltonian parameters: $A_\parallel > A_\perp$ ($A_\perp = 86$ and $A_\parallel = 193$); $g_\perp > g_\parallel$ ($g_\perp = 1.99$ and $g_\parallel = 1.93$). This suggests a square pyramidal coordination geometry, with the V=O bond aligned along the z axis and exhibiting C_{4V} symmetry [38]. The EPR spectrum of [PS-ATP-Mn] exhibits six hyperfine lines, resulting from the interaction between the electron spin and the nuclear spin of ^{55}Mn ($I = 5/2$, $2nI + 1 = 6$). The Hamiltonian parameters, $A = 74$ G and $g = 2.03$, are indicative of Mn(II) species with axial symmetry and an octahedral coordination environment [39]. The copper catalyst displays a characteristic axial spectrum with $g_\parallel > g_e$ ($g_\parallel = 2.27$), along with hyperfine splitting in the parallel region due to ^{55}Cu ($I = 3/2$, $2nI + 1 = 4$). The hyperfine lines divide the parallel component, maintaining an average separation of 122 G. The spectrum suggests that Cu(II) species are uniformly incorporated within the polymer matrix, with no evidence of Cu–Cu interactions. However, the perpendicular region of the spectrum appears unresolved. The observed g value implies that the unpaired electron in copper resides in the $d_{x^2-y^2}$ orbital. The EPR spectra of the other catalysts were not well resolved, so their EPR parameters could not be determined [40].

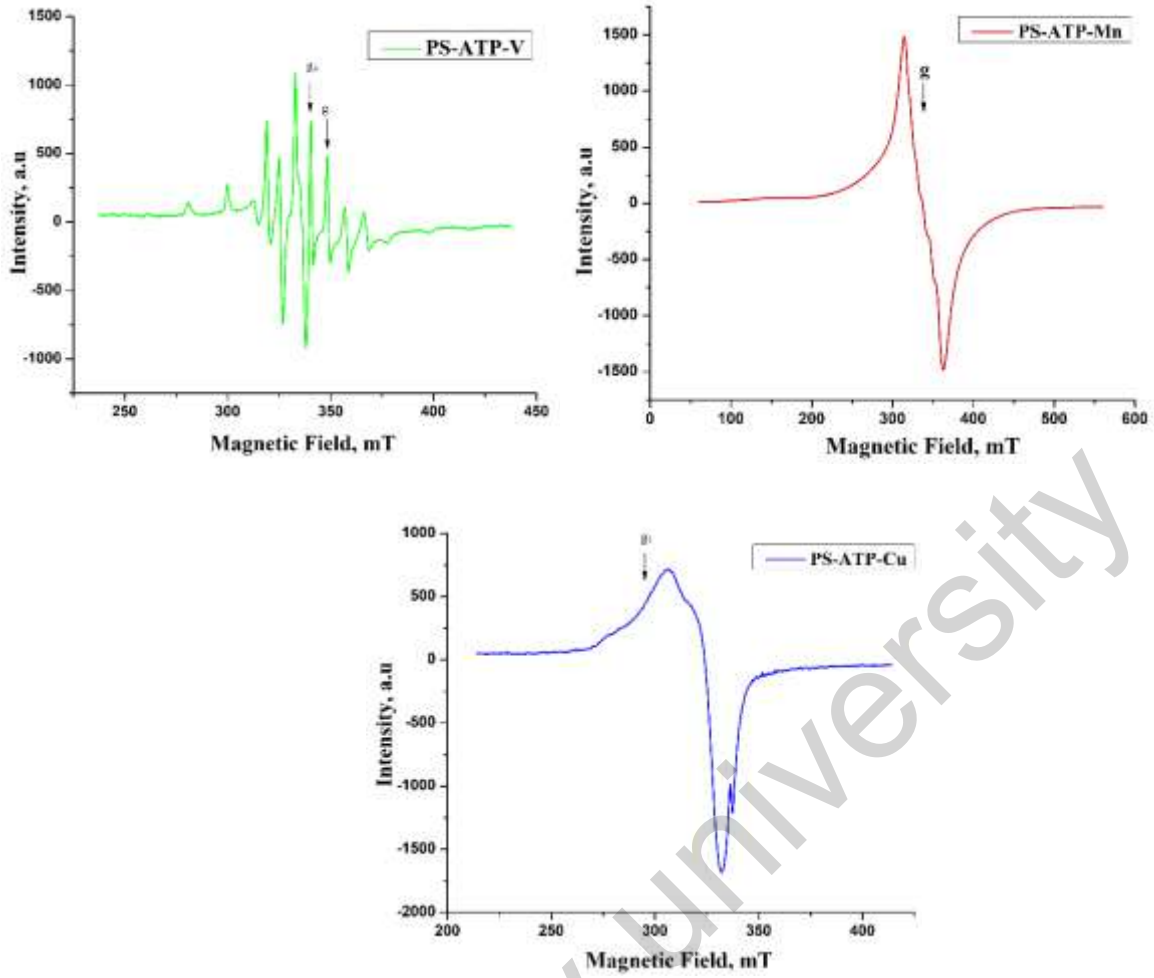

Figure 8. EPR spectra of [PS-ATP-V], [PS-ATP-Mn] and [PS-ATP -Cu]

Catalytic Performance

The catalytic performance of the synthesized materials was evaluated through the oxidation of ethylbenzene using TBHP and H_2O_2 as oxidizing agents. Control experiments confirmed that both the catalyst and the oxidant were essential for the reaction to proceed. The primary oxidation products obtained were acetophenone, benzaldehyde, and benzoic acid. To optimize the product yield, we investigated the influence of several reaction parameters, including the choice of oxidant, duration of the reaction, temperature, and catalyst dosage.

Influence of Catalyst Dosage

Figure 9 illustrates the impact of catalyst dosage on the oxidation of ethylbenzene. The data reveal that with 0.1 g of catalyst, the reaction proceeded at a slower rate, resulting in lower conversion under the given conditions. An increase in catalyst loading to 0.15 g led to a noticeable enhancement in conversion. However, further increasing the catalyst amount beyond this point did not yield any significant improvement in the oxidation process.

Influence of Oxidant

In the present work, H_2O_2 and TBHP were chosen as oxidants as they are green and environmentally benign, producing only water or tert-butanol as by-products and avoiding the use of halogenated or toxic oxidants. Preliminary trials with molecular oxygen under similar conditions resulted in very low conversion. The investigation examined how TBHP and H_2O_2 influenced the catalytic performance of polystyrene-supported catalysts in ethylbenzene oxidation. As shown in Tables 3 and 4, both oxidants facilitated a conversion rate of 53.8 % when used with the copper catalyst. Notably, the highest selectivity for acetophenone, reaching 83.9 %, was observed when H_2O_2 served as the oxidizing agent in combination with the copper catalyst.

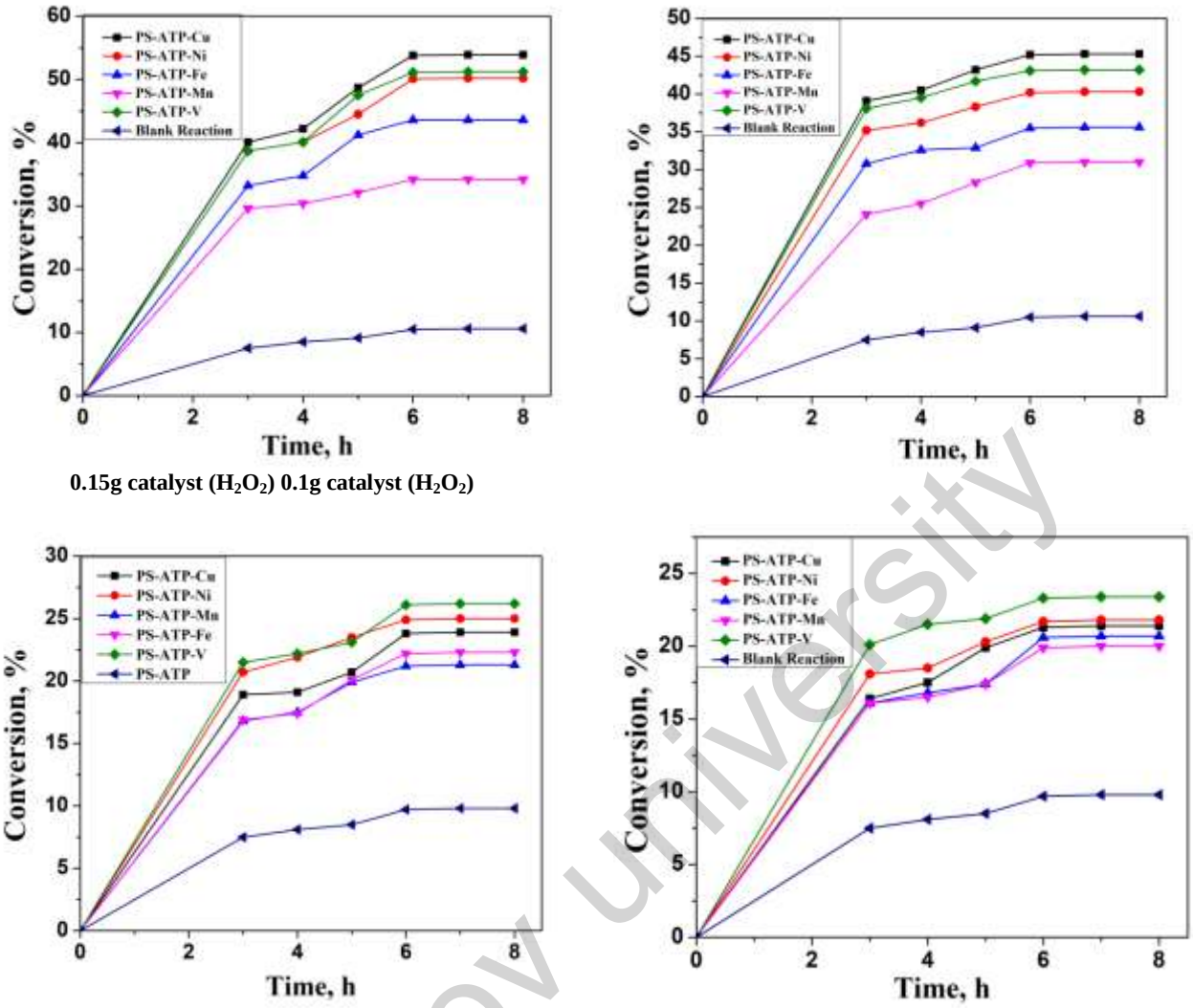

Figure 9. Influence of time on the oxidation of ethylbenzene in presence of different catalysts

Influence of Time

The reaction progress was tracked by performing ethylbenzene oxidation using a 1:2 ratio of TBHP/H_2O_2, with 0.1 g / 0.15 g of catalyst at an optimized temperature (60 °C). During the first two hours, minimal conversion was observed, suggesting an induction phase. As the reaction proceeded, ethylbenzene conversion gradually increased across all catalysts. As illustrated in Figure 9, a comparison between 3–8 hours indicated that the maximum conversion occurred at the 6-hour mark. Furthermore, product selectivity remained relatively stable despite extended reaction times.

Influence of Temperature

At room temperature, no detectable products were formed. As the temperature was increased to 60 °C, ethylbenzene conversion improved significantly. However, beyond 60 °C, no significant improvement in conversion was observed at 70 °C and 80 °C. Therefore, 60 °C was identified as the optimal temperature for maintaining both selectivity and conversion efficiency.

Table 3

Conversion of ethylbenzene and product selectivity

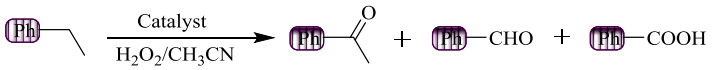

Catalysts	Catalyst concentration, g	Time, hr	Conversion, %	Selectivity, %			
							Others
Blank Reaction		3	7.5	75.8	18.1	2.5	3.6
		4	8.5	76.1	18.3	2.6	3.0
		5	9.1	77.2	18.3	2.6	1.9
		6	10.5	77.2	18.4	2.7	1.7
[PS-ATP-V]	0.1	3	38.1	66.5	21.3	2.9	9.3
		4	39.5	66.9	21.2	2.1	9.8
		5	41.7	67.1	19.8	1.9	11.2
		6	43.1	67.5	19.7	1.7	11.1
	0.15	3	38.7	66.8	19.3	2.5	11.4
		4	40.1	67.5	19.2	2.4	10.9
		5	47.5	68.3	18.9	2.1	10.7
		6	51.1	69.2	18.8	1.9	10.1
[PS-ATP-Mn]	0.1	3	24.1	62.1	22.5	3.9	11.5
		4	25.5	62.8	22.4	3.7	11.1
		5	28.3	63.1	22.1	3.7	11.1
		6	30.9	64.3	21.9	3.6	10.2
	0.15	3	29.6	62.3	21.9	3.5	12.3
		4	30.4	63.5	21.8	3.3	11.4
		5	32.1	63.9	21.5	3.2	11.4
		6	34.2	65.4	21.4	3.1	10.2
[PS-ATP-Fe]	0.1	3	30.8	68.1	21.1	3.2	7.6
		4	32.6	69.3	20.9	3.1	6.7
		5	32.9	69.7	20.7	2.9	6.7
		6	35.5	70.2	20.6	2.8	6.4
	0.15	3	33.2	69.2	20.6	2.5	7.7
		4	34.8	69.9	20.5	2.3	7.3
		5	41.2	70.9	19.9	2.3	6.9
		6	43.6	71.3	19.8	2.2	6.4
[PS-ATP-Ni]	0.1	3	35.1	78.3	17.2	1.1	3.4
		4	36.2	79.2	17.1	1.1	2.6
		5	38.3	80.3	17.1	1.2	1.4
		6	40.2	80.8	16.9	1.2	1.1
	0.15	3	38.7	78.9	14.9	1.4	4.8
		4	40.1	80.7	15.1	1.3	2.9
		5	44.5	82.4	15.1	1.3	2.9
		6	50.1	83.9	14.8	1.1	0.2
PS-ATP-Cu	0.1	3	39.1	71.2	15.6	2.7	10.5
		4	40.5	72.3	16.8	2.1	8.8
		5	43.2	72.9	16.8	2.1	8.8
		6	45.2	73.1	16.7	1.9	8.3
	0.15	3	40.1	72.5	19.1	1.5	6.9
		4	42.2	73.8	19.3	1.6	5.3
		5	48.7	74.4	19.5	1.6	4.5
		6	53.8	75.1	19.3	1.4	4.2

Reaction Condition: Acetonitrile (20 mL), ethylbenzene (10 mmol), and H_2O_2 (20 mmol) at 60 °C.

Table 4

Conversion of ethylbenzene and product selectivity

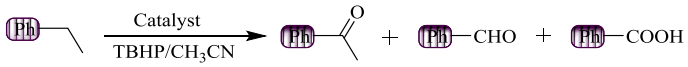

Catalysts	Catalyst concentration, g	Time, hr	Conversion, %	Selectivity, %			
					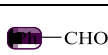	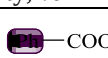	Others
Blank Reaction		3	7.5	59.1	17.2	5.1	18.6
		4	8.1	59.2	17.5	5.2	18.1
		5	8.5	59.2	17.6	5.2	18.0
		6	9.7	59.3	17.6	5.3	17.8
[PS-ATP-V]	0.1	3	20.1	65.5	18.3	4.9	11.3
		4	21.5	65.6	18.5	5.1	10.8
		5	21.9	65.6	18.5	5.2	10.7
		6	23.3	65.7	18.6	5.3	10.4
	0.15	3	21.5	65.6	18.5	5.4	10.5
		4	22.2	65.8	18.6	5.6	10.0
		5	23.1	65.9	18.9	5.3	9.9
		6	26.1	66.1	19.1	5.1	9.7
[PS-ATP-Mn]	0.1	3	16.1	58.7	21.4	3.9	16.0
		4	16.5	58.9	21.4	3.5	16.2
		5	17.4	58.9	21.5	3.3	16.3
		6	19.9	59.1	21.6	3.2	16.1
	0.15	3	16.8	58.3	21.5	4.5	15.7
		4	17.5	58.9	21.6	4.5	15.0
		5	19.9	59.2	21.8	4.7	14.3
		6	21.2	59.4	21.9	4.8	13.9
[PS-ATP-Fe]	0.1	3	16.1	68.1	21.1	3.2	7.6
		4	16.8	69.3	20.9	3.1	6.7
		5	17.4	69.7	20.7	2.9	6.7
		6	20.6	70.2	20.6	2.8	6.4
	0.15	3	16.9	69.2	20.6	2.5	7.7
		4	17.6	69.9	20.5	2.3	7.3
		5	20.1	70.9	19.9	2.3	6.9
		6	22.2	71.3	19.8	2.2	6.4
[PS-ATP-Ni]	0.1	3	16.1	67.3	16.9	6.1	9.7
		4	17.5	67.6	17.1	6.3	9.3
		5	20.3	68.1	17.2	6.4	8.3
		6	24.2	68.8	17.2	6.4	7.6
	0.15	3	20.7	67.7	14.5	3.3	14.5
		4	21.9	67.7	14.7	3.2	14.4
		5	23.5	68.9	14.7	3.2	13.2
		6	24.9	69.1	14.8	3.1	13.0
PS-ATP-Cu	0.1	3	18.1	62.1	16.5	3.7	17.7
		4	18.5	63.2	16.6	3.6	16.6
		5	19.9	63.2	16.6	3.6	16.6
		6	21.3	63.7	16.7	3.1	16.5
	0.15	3	18.9	62.3	18.1	2.6	17.0
		4	19.1	63.8	18.2	2.5	15.5
		5	20.7	63.9	18.5	2.6	15.0
		6	23.8	64.1	18.5	2.3	15.1

Reaction Condition: Acetonitrile (20 mL), ethylbenzene (10 mmol), and TBHP (20 mmol) at 60 °C.

Reusability Evaluation

The reusability of polymer-supported metal complexes in ethylbenzene oxidation was assessed. Each cycle was followed by filtration, washing, drying, and reusing of the catalysts under the same conditions. Product yields and selectivity remained stable, though a slight decline in conversion was noted after five cycles (Table 5, Figure 10). IR and DRS spectra showed no significant structural changes, indicating catalyst integrity. AAS analysis detected minor metal leaching in the fifth cycle, but overall stability ensured effective reuse, making the catalysts cost-efficient and environmentally friendly.

Table 5

Recyclability Test

Catalyst	Cycle	Conversion, %	Selectivity, %			
						Others
[PS-ATP-V]	1	51.1	69.2	18.8	1.9	10.1
	2	51.1	69.2	18.8	1.9	10.1
	3	50.0	69.2	18.8	1.9	10.1
	4	49.9	69.2	18.8	1.9	10.1
	5	49.9	69.2	18.8	1.9	10.1
[PS-ATP-Mn]	1	34.2	65.4	21.4	3.1	10.2
	2	34.1	65.4	21.4	3.1	10.2
	3	34.0	65.4	21.4	3.1	10.2
	4	33.9	65.4	21.4	3.1	10.2
	5	33.9	65.4	21.4	3.1	10.2
[PS-ATP-Fe]	1	43.6	71.3	19.8	2.2	6.4
	2	43.5	71.3	19.8	2.2	6.4
	3	43.4	71.3	19.8	2.2	6.4
	4	43.3	71.3	19.8	2.2	6.4
	5	43.3	71.3	19.8	2.2	6.4
[PS-ATP-Ni]	1	50.1	83.9	14.8	1.1	0.2
	2	50.1	83.9	14.8	1.1	0.2
	3	50.0	83.9	14.8	1.1	0.2
	4	49.9	83.9	14.8	1.1	0.2
	5	49.9	83.9	14.8	1.1	0.2
[PS-ATP-Cu]	1	53.8	75.1	19.3	1.4	4.2
	2	53.8	75.1	19.3	1.4	4.2
	3	53.7	75.1	19.3	1.4	4.2
	4	53.6	75.1	19.3	1.4	4.2
	5	53.6	75.0	19.3	1.4	4.2

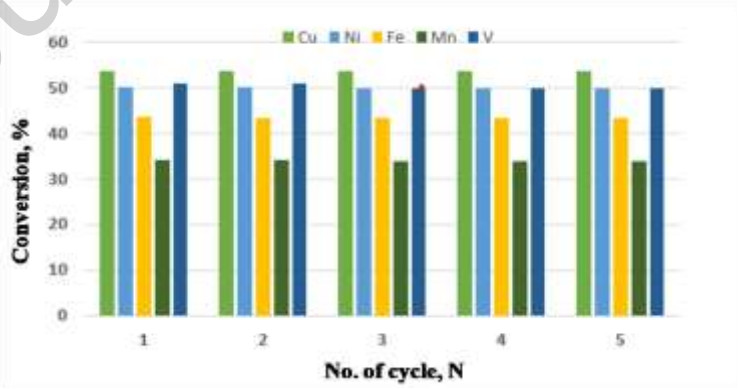

Figure 10. Recyclability test of polystyrene-anchored metal catalyst

Probable Mechanism for Oxidation of Ethylbenzene

Figure11 illustrates a proposed pathway for the oxidation of ethylbenzene using peroxides such as hydrogen peroxide or *tert*-butyl hydroperoxide (TBHP) in the presence of a metal-based catalyst. Initially, the metal catalyst interacts with the oxidant to produce a reactive hydroperoxide intermediate, accompanied by the release of counterions like chloride or acetate. This is followed by the formation of a resonance-stabilized benzylic carbocation, which undergoes a nucleophilic attack by the *tert*-butylperoxide anion. The resulting phenylethanol intermediate subsequently rearranges and experiences bond cleavage within the peroxide moiety, ultimately producing benzaldehyde and acetophenone as final oxidation products [41].

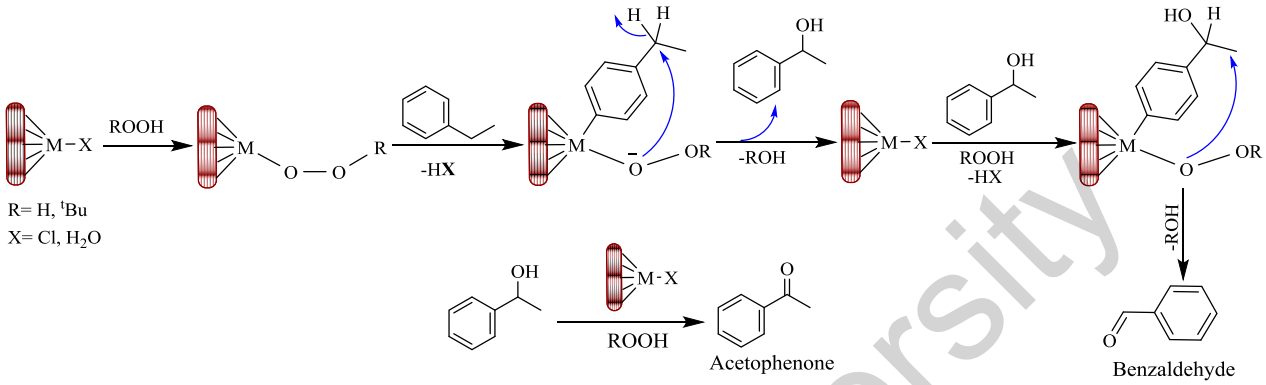

Figure 11. Proposed mechanism for the H_2O_2/TBHP facilitated oxidation of ethylbenzene catalyzed by supported catalyst

Conclusions

In summary, new catalytic systems {[PS-ATP-V], [PS-ATP-Mn], [PS-ATP-Fe], [PS-ATP-Ni], and [PS-ATP-Cu]} were developed and characterized. Their catalytic efficiency was assessed using ethylbenzene as a model substrate. Oxidation reactions were performed under optimized conditions (0.15 g catalyst, 6-hour reaction time, 60 °C) with H_2O_2 or TBHP as oxidants. Among the catalysts, [PS-ATP-Cu] exhibited the highest ethylbenzene conversion (53.8 %) with H_2O_2, whereas [PS-ATP-Mn] showed the lowest conversion (21.2 %) with TBHP. The best selectivity for acetophenone (83.9 %) was achieved using [PS-ATP-Ni] with H_2O_2, while [PS-ATP-Mn] had the lowest selectivity (59.4 %) with TBHP. These catalysts demonstrated excellent stability, maintaining their activity over five reuse cycles with minimal loss, indicating their potential for broader applications in heterogeneous catalysis.

*Author Information**

**The authors' names are presented in the following order: First Name, Middle Name and Last Name*

Savita Kumari — Research Scholar, Department of Chemistry, Maharishi Markandeshwar (Deemed to be University), Mullana, Haryana, 133207, India; e-mail: sheoransavita4@gmail.com; https://orcid.org/0009-0005-9438-2445

Praveen Kumar Gupta (*corresponding author*) — Professor, Department of Chemistry, Maharishi Markandeshwar (Deemed to be University), 133207, Mullana, Haryana, India; e-mail: praveenguptachem@gmail.com; parveen.gupta@mmumullana.org; https://orcid.org/0000-0002-2718-1310

Amit Kumar — Assistant Professor, Department of Chemistry, Indira Gandhi National College, Ladwa, Kurukshetra-136132, Haryana, India; e-mail: amitvash76@gmail.com; https://orcid.org/0009-0000-2748-1543

Ramesh Kumar — Associate Professor, Department of Chemistry, Kurukshetra University, Kurukshetra-136119, Haryana, India; e-mail: rameshkumarkuk@gmail.com; https://orcid.org/0000-0003-2089-2213

Author Contributions

The manuscript was written through contributions of all authors. All authors have given approval to the final version of the manuscript. CRediT: **Savita Kumari** writing original draft, experimentation; **Praveen Kumar Gupta** writing, review, editing, supervision; **Amit Kumar** methodology, validation, visualization; **Ramesh Kumar** software**,** formal analysis, supervision, validation.

Acknowledgments

The authors are thankful to the Maharishi Markandeshwar (Deemed to be University), Mullana, Haryana, India.

Conflicts of Interest

The authors declare no conflict of interest.

References

1 Nørskov, J. K., Studt, F., Abild-Pedersen, F., & Bligaard, T. (2014). *Fundamental concepts in heterogeneous catalysis*. John Wiley & Sons. https://doi.org/10.1002/9781118892114

2 Spargo, P. L. (2005). Transition Metals for Organic Synthesis: Building Blocks and Fine Chemicals. Second Revised and Enlarged Edition. (2-Volume Set.) Edited by Matthias Beller and Carsten Bolm. Wiley-VCH: Weinheim. 2004. 662 pp. (Vol. 1), 652 pp. (Vol. 2). £270. ISBN 3-527-30613-7. Organic Process Research & Development, 9(6), 1017–1018. https://doi.org/10.1021/op050145w

3 Ayogu, J. I., & Onoabedje, E. A. (2019). Recent advances in transition metal-catalysed cross-coupling of (hetero)aryl halides and analogues under ligand-free conditions. *Catalysis Science & Technology*, *9*(19), 5233–5255. https://doi.org/10.1039/C9CY01331H

4 Maharana, T., Nath, N., Pradhan, H. C., Mantri, S., Routaray, A., & Sutar, A. K. (2022). Polymer-supported first-row transition metal schiff base complexes: Efficient catalysts for epoxidation of alkenes. *Reactive and Functional Polymers*, *171*, 105142. https://doi.org/10.1016/j.reactfunctpolym.2021.105142

5 Sharma, A. S., Sharma, V. S., Yadav, P., Kaur, H., & Varma, R. S. (2023). Polystyrene Resins: Versatile and Economical Support for Heterogeneous Nanocatalysts in Sustainable Organic Reactions. *ChemCatChem*, *15*(8), e202201493. https://doi.org/10.1002/cctc.202201493

6 Wang, K., Horlyck, J., An, N., & Voutchkova-Kostal, A. (2024). Homogeneous vs. heterogeneous catalysts for acceptorless dehydrogenation of biomass-derived glycerol and ethanol towards circular chemistry. *Green Chemistry*, *26*(7), 3546–3564. https://doi.org/10.1039/D3GC04378A

7 Kumari, S., Kumar, S., Karan, R., Bhatia, R., Kumar, A., Rawal, R. K., & Gupta, P. K. (2024). Synthetic and catalytic perspectives of polystyrene supported metal catalyst. *Journal of the Iranian Chemical Society*, *21*(4), 951–1010. https://doi.org/10.1007/s13738-024-02970-7

8 Corain, B., Zecca, M., Canton, P., & Centomo, P. (2010). Synthesis and catalytic activity of metal nanoclusters inside functional resins: an endeavour lasting 15 years. *Philosophical Transactions of the Royal Society A: Mathematical, Physical and Engineering Sciences*, *368*(1915), 1495–1507. https://doi.org/10.1098/rsta.2009.0278

9 Sharma, A. S., Sharma, V. S., Yadav, P., Kaur, H., & Varma, R. S. (2023). Polystyrene Resins: Versatile and Economical Support for Heterogeneous Nanocatalysts in Sustainable Organic Reactions. *ChemCatChem*, *15*(8), e202201493. https://doi.org/10.1002/cctc.202201493

10 Králik, M., & Biffis, A. (2001). Catalysis by metal nanoparticles supported on functional organic polymers. *Journal of Molecular Catalysis A: Chemical*, *177*(1), 113–138. https://doi.org/10.1016/s1381-1169(01)00313-2

11 Azeez, M. O., Nafiu, S. A., Olarewaju, T. A., Olabintan, A. B., Tanimu, A., Gambo, Y., & Aitani, A. (2023). Selective catalytic oxidation of ethylbenzene to acetophenone: a review of catalyst systems and reaction mechanisms. *Industrial & Engineering Chemistry Research*, *62*(33), 12795–12828. https://doi.org/10.1021/acs.iecr.3c01588

12 Siddiqi, I., & Pitre, K. S. (2003). Determination of phenones in a perfume composition. *Reviews in Analytical Chemistry*, *22*(1), 9–18. https://doi.org/10.1515/REVAC.2003.22.1.9

13 Kizilcan, N., Galioğlu, O., & Akar, A. (1993). Modified cyclohexanone – formaldehyde and acetophenone – formaldehyde resins. *Journal of applied polymer science*, *50*(4), 577–584. https://doi.org/10.1002/app.1993.070500402

14 Zubkov, F. I., & Kouznetsov, V. V. (2023). Traveling across life sciences with acetophenone — a simple ketone that has special multipurpose missions. *Molecules*, *28*(1), 370. https://doi.org/10.3390/molecules28010370

15 Soucy, N. V. (2014). Acetophenone. *Encyclopedia of Toxicology*, 43–45. https://doi.org/10.1016/b978-0-12-386454-3.01157-x

16 Mohammadi Ziarani, G., Kheilkordi, Z., & Mohajer, F. (2020). Recent advances in the application of acetophenone in heterocyclic compounds synthesis. *Journal of the Iranian Chemical Society*, 17, 247–282. https://doi.org/10.1007/s13738-019-01774-4

17 Loch, C., Reusch, H., Ruge, I., Godelmann, R., Pflaum, T., Kuballa, T., & Lachenmeier, D. W. (2016). Benzaldehyde in cherry flavour as a precursor of benzene formation in beverages. *Food Chemistry*, 206, 74–77. https://doi.org/10.1016/j.foodchem.2016.03.034

18 Opgrande, J. L., Dobratz, C. J., Brown, E., Liang, J., Conn, G. S., Shelton, F. J., & With, J. (2000). *Benzaldehyde*. Kirk-Othmer Encyclopedia of Chemical Technology. https://doi.org/10.1002/0471238961.0205142615160718.a01

19 Mohammadi, A., Mohammadi, S., Bayandori Moghaddam, A., Masoumi, V., & Walker, R. B. (2014). Electropolymerized fluorinated aniline-based fiber for headspace solid-phase microextraction and gas chromatographic determination of benzaldehyde in injectable pharmaceutical formulations. *Journal of chromatographic science*, *52*(9), 971–976. https://doi.org/10.1093/chromsci/bmt152

20 Theodoropoulou, M. A., Nikitas, N. F., & Kokotos, C. G. (2020). Aldehydes as powerful initiators for photochemical transformations. *Beilstein Journal of Organic Chemistry*, *16*(1), 833–857. https://doi.org/10.3762/bjoc.16.76

21 Sieber, R., Bütikofer, U., & Bosset, J. O. (1995). Benzoic acid as a natural compound in cultured dairy products and cheese. *International Dairy Journal*, *5*(3), 227–246. https://doi.org/10.1016/0958-6946(94)00005-A

22 Londry, K. L., & Fedorak, P. M. (1992). Benzoic acid intermediates in the anaerobic biodegradation of phenols. *Canadian Journal of Microbiology*, *38*(1), 1–11. https://doi.org/10.1139/m92-001

23 Faraji, A. R., Mosazadeh, S., & Ashouri, F. (2017). Synthesis and characterization of cobalt-supported catalysts on modified magnetic nanoparticle: green and highly efficient heterogeneous nanocatalyst for selective oxidation of ethylbenzene, cyclohexene and oximes with molecular oxygen. *Journal of Colloid and Interface Science*, 506, 10–26. https://doi.org/10.1016/J.JCIS.2017.06.100

24 Gao, L., Zhuge, W., Feng, X., Sun, W., Sun, X., & Zheng, G. (2019). Co/rgo synthesized via the alcohol-thermal method as a heterogeneous catalyst for the highly efficient oxidation of ethylbenzene with oxygen. *New Journal of Chemistry*, *43*(21), 8189–8194. https://doi.org/10.1039/C9NJ00470J

25 Li, J., Zhao, S., Yang, S., Wang, S., Sun, H., Jiang, S. P., Johannessen, B., & Liu, S. (2021). Atomically dispersed cobalt on graphitic carbon nitride as a robust catalyst for selective oxidation of ethylbenzene by peroxymonosulfate. *Journal of Materials Chemistry A*, 9, 3029–3035. https://doi.org/10.1039/d0ta11503g

26 Yamazaki, S. (1999). Chromium (VI) oxide-catalyzed benzylic oxidation with periodic acid. *Organic Letters*, *13*(1), 2129–2132. https://doi.org/10.1021/ol991175k

27 Yang, Y., Zhong, W., Nie, B., Chen, J., Wei, Z., & Liu, X. (2017) Synergetic oxidation of ethylbenzene to acetophenone catalyzed by manganese(II) complexes bearing pendant iodophenyl groups. *Journal of Organometallic Chemistry*, 853, 136–142. https://doi.org/10.1016/J.JORGANCHEM.2017.10.034

28 Venkatesh, G., Vennila, P., Kaya, S., Ahmed, S. B., Sumathi, P., Siva, V., & Kamal, C. (2024). Synthesis and spectroscopic characterization of Schiff base metal complexes, biological activity, and molecular docking studies. *ACS omega*, *9*(7), 8123–8138. https://doi.org/10.1021/acsomega.3c08526

29 Raman, N., Kulandaisamy, A., & Jeyasubramanian, K. (2001). Synthesis, spectroscopic characterization, redox, and biological screening studies of some Schiff base transition metal (II) complexes derived from salicylidene-4-aminoantipyrine and 2-aminophenol/2-aminothiophenol. *Synthesis and Reactivity in Inorganic and Metal-Organic Chemistry*, *31*(7), 1249–1270. https://doi.org/10.1081/SIM-100106862

30 Islam, M. T., Bitu, M. N. A., Ali, M. A., Hossen, M. F., & Kudrat, M. (2024). Oxovanadium (IV) complexes of α-Amino acid schiff bases and 2,2′-Bipyridine ligands: Synthesis, characterization and investigation of their biological potency. http://dx.doi.org/10.52711/0974-4150.2024.00020

31 Aly, A. A., Ghandour, M., & Alfakeh, M. S. (2012). Synthesis and characterization of transition metal coordination polymers derived from 1,4-benzenedicarboxylate and certain azoles. *Turkish Journal of Chemistry*, *36*(1), 69–79. https://doi.org/10.3906/kim-1106-61

32 Al-Fakeh, M. S. (2020). Synthesis, thermal stability and kinetic studies of copper (II) and cobalt (II) complexes derived from 4-aminobenzohydrazide and 2-mercaptobenzothiazole. *European Chemical Bulletin*, *9*(12), 403–409. http://dx.doi.org/10.17628/ecb.2020.9.403-409

33 Maurya, M. R., Chauhan, A., Arora, S., & Gupta, P. (2022). Triazole based oxidovanadium (V) complex supported on chloromethylated polymer and its catalytic activity for the synthesis of dihydropyrimidinones (DHPMs). *Catalysis Today*, 397, 3–15. https://doi.org/10.1016/j.cattod.2022.03.006

34 Gomathi, V., & Selvameena, R. (2022). Synthesis, structural analysis and antimicrobial screening of Mn (II) complexes of Schiff bases. *Journal of the Mexican Chemical Society*, *66*(1), 70–78. https://doi.org/10.29356/jmcs.v66i1.1621

35 Buldurun, K., Turan, N., Savci, A., Alan, Y., & Colak, N. (2022). Synthesis, characterization, X-ray diffraction analysis of a tridentate Schiff base ligand and its complexes with Co (II), Fe (II), Pd (II) and Ru (II): Bioactivity studies. *Iran. J. Chem. Chem. Eng.*, *41*(8). https://doi.org/10.30492/ijcce.2021.531629.4775

36 Dinku, D., Demissie, T. B., Beas, I. N., Eswaramoorthy, R., Abdi, B., & Desalegn, T. (2024). Antimicrobial activities and docking studies of new Schiff base ligand and its Cu (II), Zn (II) and Ni (II) Complexes: Synthesis and Characterization. *Inorganic Chemistry Communications*, 160, 111903. https://doi.org/10.1016/j.inoche.2023.111903

37 Chellaian, J. D., & SS, S. R. (2021). Co (II), Ni (II), Cu (II), and Zn (II) complexes of 4-aminoantipyrine-derived Schiff base. Synthesis, structural elucidation, thermal, biological studies, and photocatalytic activity. *Journal of Heterocyclic Chemistry*, *58*(4), 928–941. https://doi.org/10.1002/jhet.4209

38 Vijayan, J. G. (2022). Synthesis, Characterization, Magnetic, Thermal and Electrochemical Studies of Oxovanadium (IV) Complex of 2-thiophenecarba Benzhydrazone. In *Advanced Polymeric Materials* (pp. 59–72). River Publishers. https://doi.org/10.1201/9781003337041-3

39 Mureseanu, M., Filip, M., Bleotu, I., Spinu, C. I., Marin, A. H., Matei, I., & Parvulescu, V. (2023). Cu (II) and Mn (II) Anchored on Functionalized Mesoporous Silica with Schiff Bases: Effects of Supports and Metal–Ligand Interactions on Catalytic Activity. *Nanomaterials, 13*(12), 1884. https://doi.org/10.3390/nano13121884

40 Howsaui, H. B., Sharfalddin, A. A., Abdellattif, M. H., Basaleh, A. S., & Hussien, M. A. (2021). Synthesis, spectroscopic characterization and biological studies of Mn (II), Cu (Ii), Ni (II), Co (II) and Zn (II) complexes with new schiff base of 2-((pyrazine-2-ylimino)methyl) phenol. *Applied Sciences, 11*(19), 9067. https://doi.org/10.3390/app11199067

41 Azeez, M. O., Nafiu, S. A., Olarewaju, T. A., Olabintan, A. B., Tanimu, A., Gambo, Y., & Aitani, A. (2023). Selective catalytic oxidation of ethylbenzene to acetophenone: a review of catalyst systems and reaction mechanisms. *Industrial & Engineering, 62*(33), 12795–12828. https://doi.org/10.1021/acs.iecr.3c01588